8-2014

Modeling of Power Spectral Density of Modified von Karman Atmospheric Phase Turbulence and Acousto-Optic Chaos using Scattered Intensity Profiles over Discrete Time Intervals

Monish Ranjan Chatterjee
University of Dayton, mchatterjee1@udayton.edu

Fathi H.A. Mohamed
University of Dayton

Modeling of Power Spectral Density of Modified von Karman Atmospheric Phase Turbulence and Acousto-Optic Chaos Using Scattered Intensity Profiles Over Discrete Time Intervals

Monish R. Chatterjee[1,*] and Fathi H. A. Mohamed[1]

[1]Department of Electrical & Computer Engineering

University of Dayton, Dayton, Ohio 45469

[*]Corresponding author

ABSTRACT

In recent research, propagation of plane electromagnetic (EM) waves through a turbulent medium with modified von Karman phase characteristics was modeled and numerically simulated using transverse planar apertures representing narrow phase turbulence along the propagation path. The case for extended turbulence was also studied by repeating the planar phase screens multiple times over the propagation path and incorporating diffractive effects via a split-step algorithm. The goal of the research reported here is to examine two random phenomena: (a) atmospheric turbulence due to von Karman-type phase fluctuations, and (b) chaos generated in an acousto-optic (A-O) Bragg cell under hybrid feedback. The latter problem has been thoroughly examined for its nonlinear dynamics and applications in secure communications. However, the statistical characteristics (such as the power spectral density (PSD)) of the chaos have not been estimated in recent work. To that end, treating the chaos phenomena as a random process, the time waveforms of the chaos intensity and their spectra are numerically evaluated over a (large) number of time iterations. These spectra are then averaged to derive the equivalent PSD of the A-O chaos. For the turbulence problem, an optical beam passing through an input pinhole is propagated through a random phase screen (placed at different locations) to a desired distance (typically near-field) under different levels of turbulence strength. The resulting spatial intensity profile is then averaged and the process repeated over a (large) number of pre-specified time intervals. From this data, once again, the turbulence PSD is calculated via the Fourier spectra of the average intensity snapshots. The results for the two systems are compared.

Keywords: von Karman model; atmospheric turbulence; inner scale; outer scale; near-field diffraction; random phase screen; planar aperture; acousto-optic chaos; nonlinear dynamics; chaotic encryption; power spectral density.

1. BACKGROUND

Atmospheric turbulence affects optical systems that operate in various atmospheric conditions. The characteristics of the optical wave transmitted through atmospheric turbulence can undergo dramatic changes resulting in degradation of system performance. Atmospheric turbulence causes index of refraction inhomogeneities such as different size eddies which affect optical wave propagation through the atmosphere. These refractive index inhomogeneities cause fluctuations in both the intensity and the phase of the received signal [1,2]. In the classical atmospheric turbulence theory, the refractive index structure parameter is the key parameter known to describe the strength of the atmospheric turbulence and accurate measurement of this parameter represents an important task. The optical property of the medium often referred to is the index of refraction. The refractive index is typically dependent on wavelength of the incident radiation and the density of the medium [3-5]. In several cases, turbulence is modeled via random phase screens that are either localized or extended over a physical space representing the turbulent medium. Recently, atmospheric turbulence

Laser Communication and Propagation through the Atmosphere and Oceans III, edited by Alexander M. J. van Eijk, Christopher C. Davis, Stephen M. Hammel, Proc. of SPIE Vol. 9224, 922404
 · doi: 10.1117/12.2065421

was modeled using the PSD of the refractive index. Included among these models are the Kolmogorov, Tatarski, von Karman, and modified von Karman spectra. The refractive index structure parameter was first introduced in the turbulence theory developed by Kolmogorov and Obukhov [2-4]. The key assumptions of classical (Kolmogorov) turbulence theory, such as statistical homogeneity and isotropy of the refractive index random field, are not always satisfied. This theory is now commonly referred to as the Kolmogorov turbulence theory [6-8]. The refractive index structure parameter describes the strength of the refractive index fluctuations and marks the first major principle on which the development of the classical Kolmogorov atmospheric turbulence theory depends [9].

In this paper, we have studied the effect of atmospheric turbulence on the propagation of the Gaussian beam profile. A brief review of the modified von Karman spectrum (MVKS) is carried out relative to narrow and extended (wide) turbulence to mimic the random statistical behavior of the atmospheric turbulence. This is done by using the MVKS random phase screen(s). Two scenarios are followed to represent the atmospheric turbulence (a) single random phase screen where the random phase screen is located at a particular distance from the aperture plane and thereafter the field intensity at the observation (image) plane is calculated; and (b) extended (multiple) random turbulence whereby a certain number of random phase screens are placed equally spaced along the propagation path separated by infinitesimal distances (Δz) and again the field intensities at different positions at the image plane are also calculated. In the case of narrow turbulence, the field is evaluated at the image plane ($z = L$) for two different turbulence conditions (weak and strong), while for wide turbulence, the propagated EM filed is measured at half of the propagation distance ($z = 0.5\ L$) for two different turbulence conditions (weak and strong). The other parameters (structure constant, Gaussian beam waist, propagation distance, and the incremental distance Δz for extended phase screen) are kept constant during propagation. More details about these parameters will be discussed in the next section. The split-step propagation method (SSPM) involving the Fresnel-Kirchhoff diffraction integral is used to model the propagation of the EM wave through turbulent medium where the propagated EM beam alternatively passes through a purely diffractive region (absence of inhomgenenties) and propagation through a non-diffractive inhomogenous medium (random phase screen in our case). This work essentially originated with the study of the propagation of the EM chaotic waves through atmospheric turbulence and utilization of such chaos in encrypting the chaotic carrier with RF information signals which were then transmitted and subsequently recovered using a set of matched keys (system parameters). One essential feature of the A-O chaos wave is that it is generated in the feedback loop containing the photodetector. As a consequence, the chaos that results (both in the photocurrent and the scattered light) is inherently time-dependent (and not a function of space). Therefore, it becomes necessary to obtain a workable time-domain turbulence model (beginning with the spatial von Karman model discussed in this document) for amplitude and/or phase that may then be incorporated in the chaotic propagation problem. A possible approach to such modeling would be to establish via the chaotic time waveforms and corresponding time-frequency PSD of the chaos under investigation. From this perspective, it has been suggested [10] that in order to check the effect of the atmospheric turbulence on propagated chaotic waves, one needs to derive the PSD for the generated chaos and the atmospheric turbulence separately. Then criteria need to be established allowing measurement of the combined influence of the turbulence and chaos (two independent statistically random phenomena) on the propagation of EM waves. In the foreseeable future, our goal will be to accordingly develop a workable PSD of narrow (or extended) turbulence based on the modified von Karman phase model. Alongside, the PSD of the chaos generated from the A-O feedback system will be derived using numerical statistics obtained from the chaos data. Eventually, the objective is to derive independent time-frequency PSDs for both chaos and (initially) narrow turbulence, followed by the derivation of the combined effect in terms of the equivalent PSD of the system, and finally examine the effect of these two processes on the propagation characteristics of EM waves (with or without modulation).

The organization of this paper is as follows: in section 2, a brief review on the modified von Karman turbulence model is presented including narrow and wide turbulence regions. Time statistical of a chaos and its PSD are reported in section 3. Derivation of the PSD of the atmospheric turbulence using a single phase screen is described in section 4. Finally, concluding remarks and ideas for possible future extensions are presented in section 5.

2. REVIEW OF VON KARMAN MODELING

Von Karman modified the Tatarski spectrum such that it is finite for $k < 1/L_0$ to make it valid over both the inner and outer scale parameters. The power spectrum density of the von Karman Spectrum (also called the modified von Karman spectrum (MVKS)) is given by [1]:

$$\Phi_n(k) = 0.033\, C_n^2\, \frac{\exp\left(-\frac{k^2}{k_m^2}\right)}{\left(k^2+k_o^2\right)^{\frac{11}{6}}} \quad , \; 0 \leq k \ll \infty \tag{1}$$

where C_n^2 is the medium structure constant, $k_m = {}^{5.92}/_{l_o}$ is an equivalent wavenumber related to the inner scale, $k_0 = {}^{2\pi}/_{L_o}$ is a wavenumber related to the outer scale, and k is the unbounded non-turbulent wave number in the medium. In the above equation, $\Phi_n(k)$ represents the so-called power spectral density (PSD) of the refractive index of the medium. Also, the main advantages of this model that it includes inner and outer scales, and it's integrable when k=0.

In this section, we discuss (in brief) the propagation of the EM waves through narrow and extended (wide) atmospheric turbulence.

2.1 Narrow turbulence

As mentioned above, some of the simulation results reported here use a narrow random phase screen placed at z = 0; the field is then evaluated at the image plane (at z = L). We will examine the propagated Gaussian beam passing through weak and strong turbulent regions. Then the 3D Gaussian beam, transverse (2D) Gaussian beam, Gaussian beam profile, random phase screen profile, and Gaussian beam phase angle are evaluated at the image plane (z = L) as shown in the following figures.

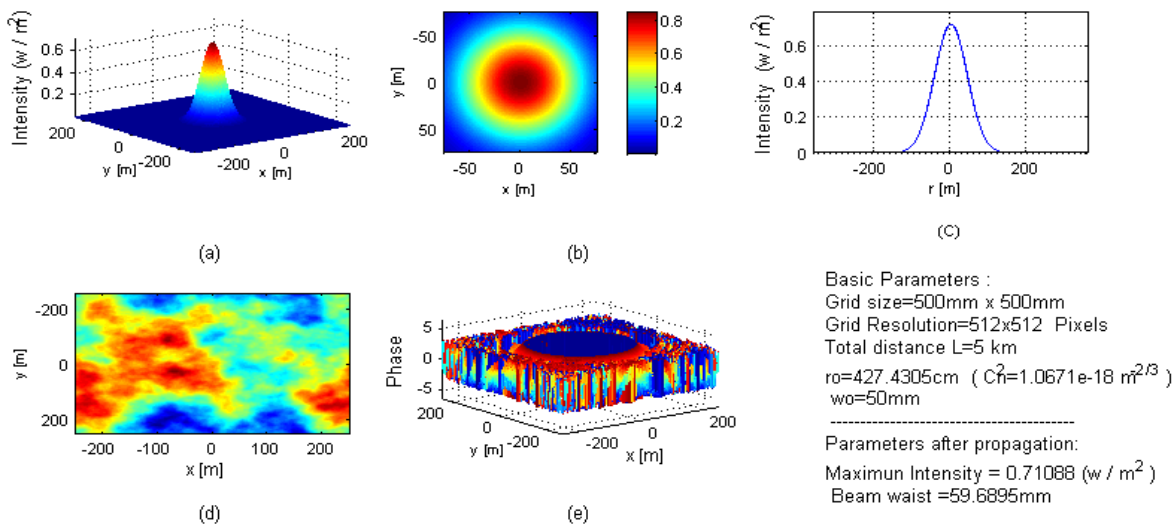

Fig.1. Gaussian beam propagation through weak turbulence to distance z=L (phase screen at the object plane). (a) 3D Gaussian beam, (b) its transverse plane intensity distribution, (c) 2D intensity profile, (d) random phase screen distribution profile, and (e) 3D field phase angle distribution in output plane.

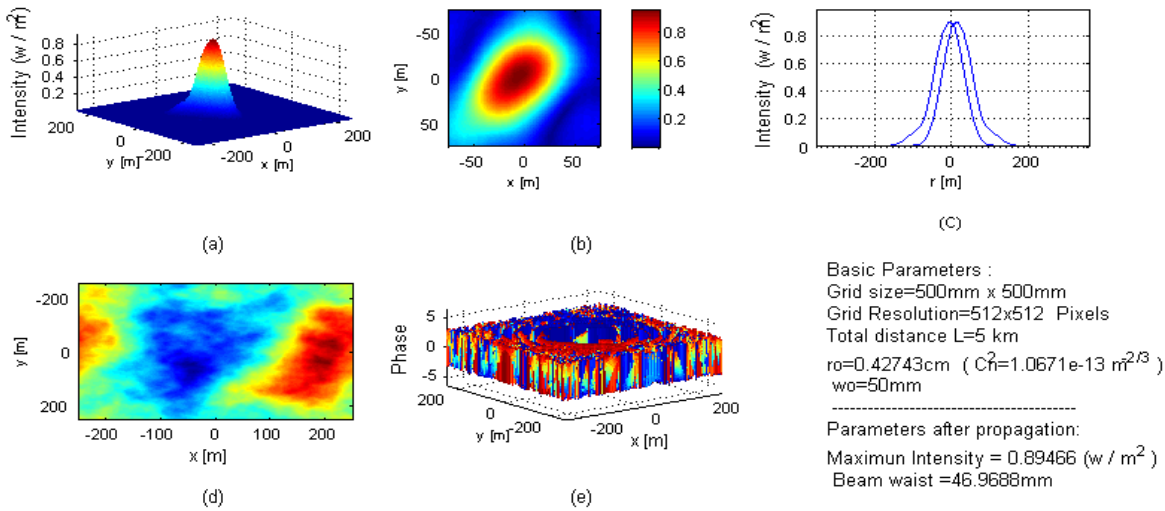

Fig.2. Gaussian beam propagation through strong turbulence to distance z=L (phase screen at the object plane). (a) 3D Gaussian beam, (b) its transverse plane intensity distribution, (c) 2D intensity profile, (d) random phase screen distribution profile, and (e) 3D field phase angle distribution in output plane.

In general, from the Figs.1 and 2, we observe that as expected the Gaussian beam suffers more distortion and more phase fluctuations in the case of strong turbulence rather than weak turbulence. Also, the strong turbulence cause greater beam splitting than in the case of weak turbulence as illustrated in Fig. 1 (c) and 2 (c). In addition, we notice that the intensity of the propagated Gaussian beam is not impacted much by turbulence compared with phase fluctuations. Therefore, it may be concluded that atmospheric turbulence has greater effect on the phase than on the intensity.

2.2 Wide turbulence

In this part, we have investigated the propagation of the EM beam through weak and strong wide turbulence region where multiple random phase screens are used to represent the statistical behavior of the atmospheric turbulence. The number of phase screens used is governed by the incremental distance Δz and the entire propagation path. The number of random phase screens used in this case is 500. A 3D profiled Gaussian beam, transverse (2D) Gaussian beam, Gaussian beam profile, random phase screen profile, and Gaussian beam phase angle are evaluated at $z = 0.5$ L (half way), as illustrated in the following figures.

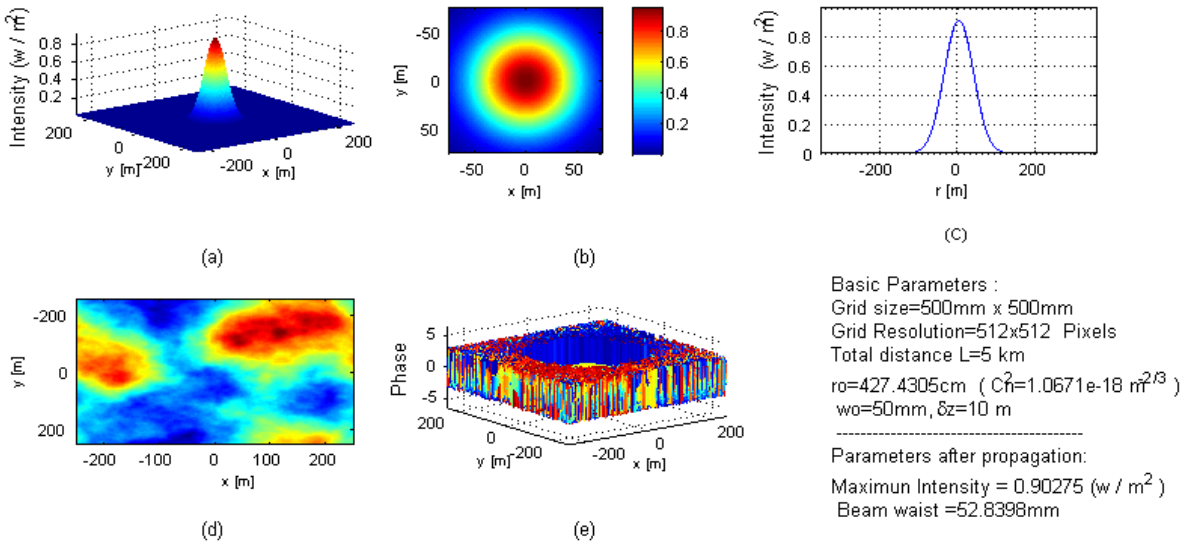

Fig. 3. Gaussian beam propagation through weak turbulence to distance Z=0.5 L (250 Δz). (a) 3D Gaussian beam, (b) its transverse plane intensity distribution, (c) 2D intensity profile, (d) random phase screen distribution profile, and (e) 3D field phase angle distribution in output plane.

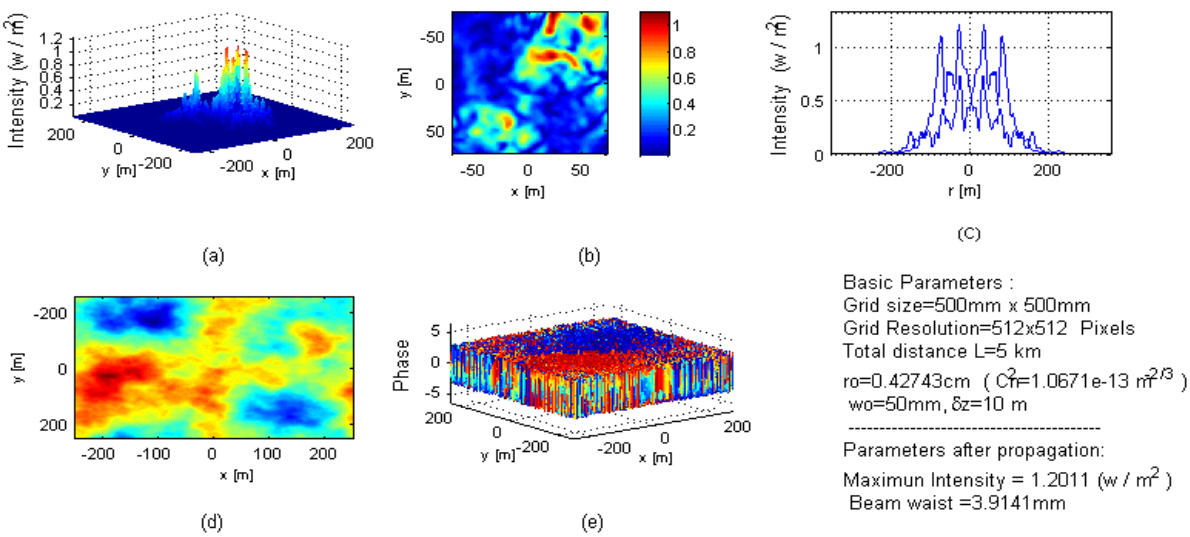

Fig. 4. Gaussian beam propagation through strong turbulence to distance Z=0.5 L (250 Δz). (a) 3D Gaussian beam, (b) its transverse plane intensity distribution, (c) 2D intensity profile, (d) random phase screen distribution profile, and (e) 3D field phase angle distribution in output plane.

Again, from Figs. 3 and 4, strong turbulence distorts the signal more than weak turbulence. This simply because multiple random phase screens (N ≈ 500) are used, so greater signal degradation is expected. Also, the phase fluctuations in the case of strong turbulence is more pronounced than in the case of weak turbulence as shown in Figs. 3(e) and 4(e).

3. ACOUSTO-OPTIC(A-O) CHAOS AND ITS POWER SPECTRAL DENSITY

3.1 A-O chaos overview

Acousto-optics, where acousto implies sound and optics implies light defines the diffraction of monochromatic light waves by ultrasonic waves whereby the monochromatic light passages through a rectangular structured cell and emerging them from the other side [11,12]. In the case of homogeneous and isotropic medium, there is no deviation in the monochromatic light through the medium. But when the medium is traversed under high-frequency sound wave (also called a grating), the light wave is diffracted. Through the action of a piezoelectric transducer, electrical signals are converted into sound waves propagating in the medium. The ultrasonic wave propagating through a solid or liquid locally causes compression and rarefaction of the medium. These compression and rarefaction effects cause perturbations in the index of refraction of the medium, which in terms creates a phase grating in the material and splits the incident laser light into various diffracted orders. Because the sound wave is sinusoidal in nature, the compressions and rarefactions in the medium are periodic in nature. When the monochromatic incident light passes through the medium at an angle called the Bragg angle (θ_B), and the grating is considered to be thick, the light is typically diffracted into two orders (called the Bragg regime), the diffracted light (first-order) and the undiffracted light (zeroth-order) [13,14,15].

In this paper, we consider the Bragg regime and will deal with the first-order diffraction. In the Bragg regime, the incident light is diffracted into the zeroth- and first-orders. The resulting first order is picked up by a linear photo detector at the output, amplified and then fed back to the adder in the feedback loop. The adder adds the feedback with the dc bias input and feeds it to the RF source that generates the RF input which is then incident on the Bragg cell via a transducer. The standard Bragg cell transmitter with feedback is shown in Fig.5.

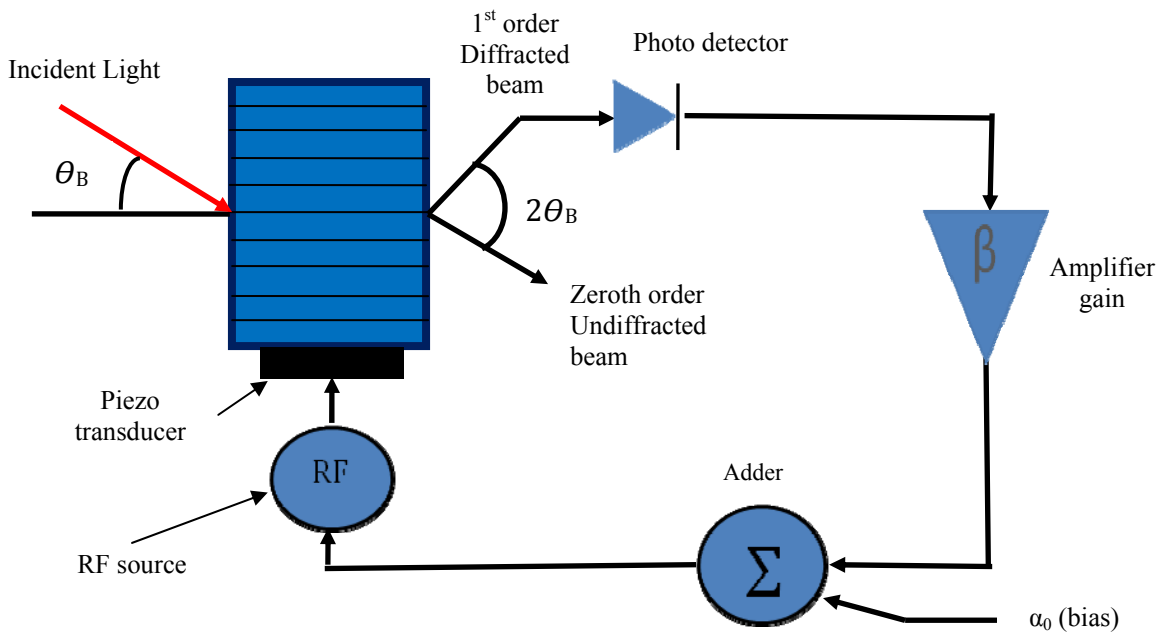

Fig.5. An A-O modulator with first-order feedback in the Bragg regime.

The first-order detected intensity follows this nonlinear dynamical equation:

$$I_1(t) = I_{inc} \sin^2\left[\frac{1}{2}\left(\hat{\alpha}_0(t) + \tilde{\beta}\, I_1(t - TD)\right)\right], \tag{2}$$

where $\hat{\alpha}_0$ is the peak phase delay through the medium, $\tilde{\beta}$ is the effective feedback gain, I_{inc} is the incident intensity, and TD is the feedback time delay including photo detector conversion delay. Under certain values of the three parameters mentioned above, the system can be driven through a series of dynamical regimes, namely, monostable, bistable, multistable, and chaos.

3.2 Chaos power spectral density

In this subsection, we will find the PSD associated with a chaotic signal for different values of time delay (TD). The values of $\tilde{\beta}$ =4, $\hat{\alpha}_0$ =2, and I_{inc} =1 are kept constant as show in each figure. Detailed definitions of the symbols stated may be found in [11].

The procedure for finding the chaos PSD adopted here is as follows:

1) Assign chosen values to the key chaos parameters as shown in each of the following figures.
2) Carry out the statistical calculations for different (fixed) vales of the time delay, TD.
3) Run the program multiple times (say 100) for given fixed parameters (thus we obtain 100 snapshots of chaos).
4) For each time waveform we compute the Fourier transform.
5) For the all Fourier transforms (100 graphs), we find the power associated with different values of frequencies (including the frequencies associated with the highest intensity), assuming hypothetically that the field intensity is collected over a fixed area over which the profile is approximately constant.
6) We compute the average transformed intensity over the 100 spectral waveforms, and finally plot the derived average spectral densities over the chosen frequency range. This should approximately result in an equivalent PSD for the chaos wave.

In the following figures (6-13), we show the snapshot of the one of the time waveforms, its Fourier transform and the PSD for different values of time delay (TD= 1ms, 100 μs, 10 μs, and 5 μs) .

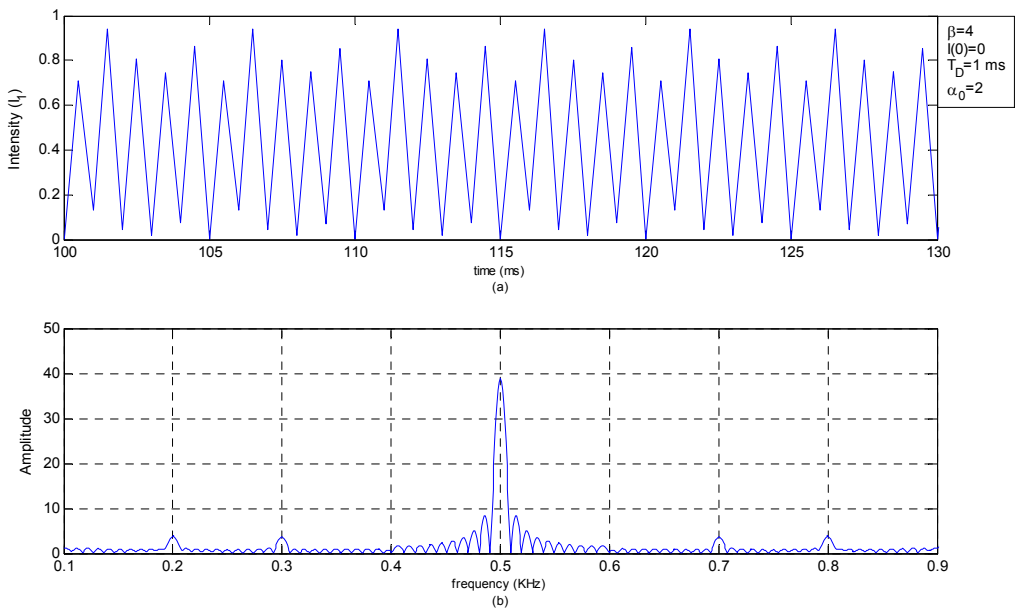

Fig.6. Chaotic wave data for (a) snapshot of time waveform, and (b) the Fourier transform.

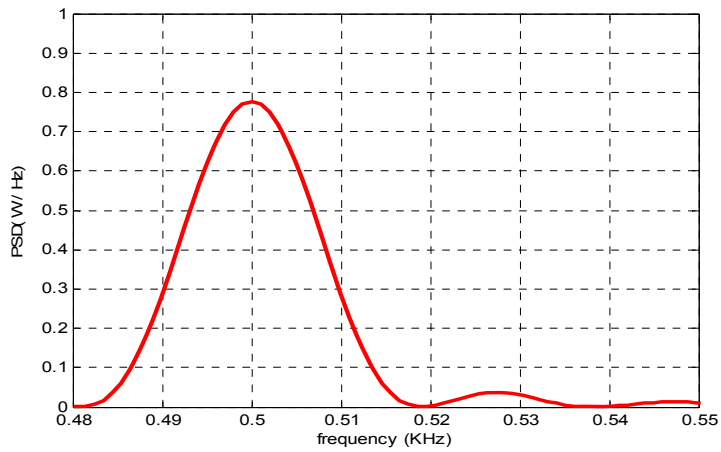

Fig.7. Chaotic wave PSD for $\tilde{\beta}$ = 4, $\hat{\alpha}_0$ = 2, I_{inc} =1, and TD = 1ms.

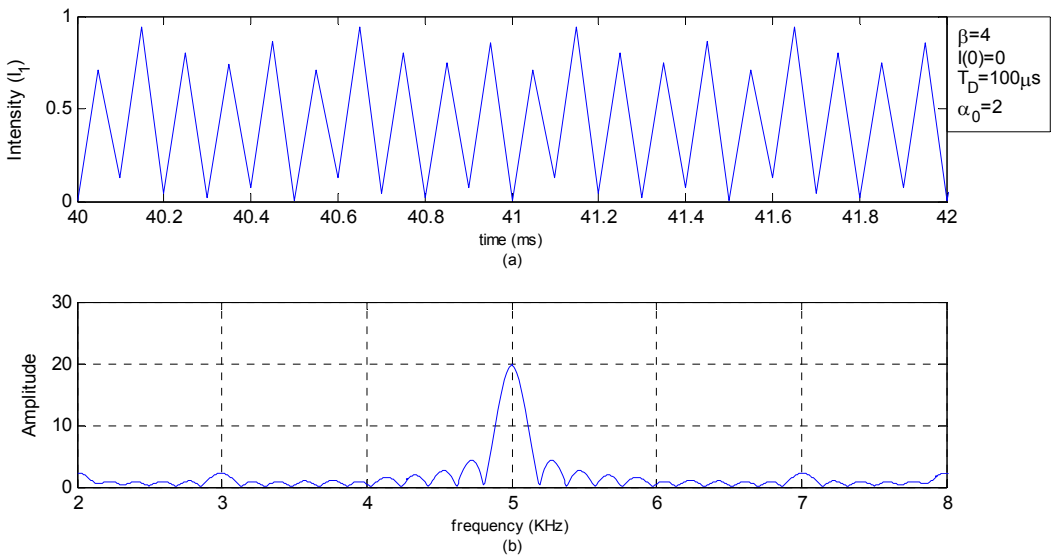

Fig.8. Chaotic wave data for (a) snapshot of time waveform, and (b) the Fourier transform.

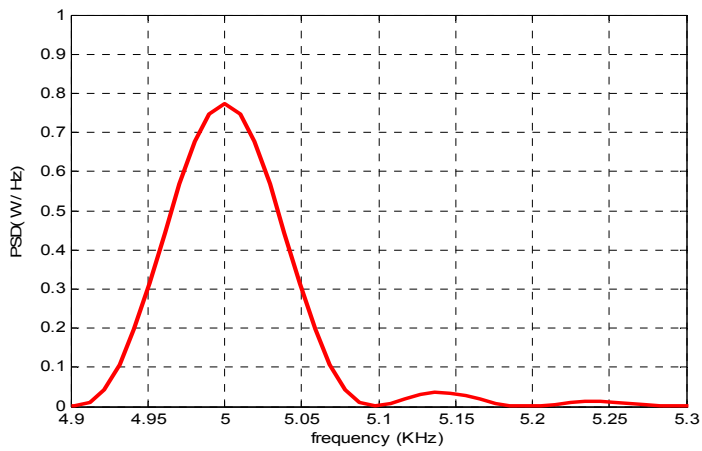

Fig.9. Chaotic wave PSD for for $\tilde{\beta}$ = 4, $\hat{\alpha}_0$ = 2, I_{inc} =1, and TD = 100μs.

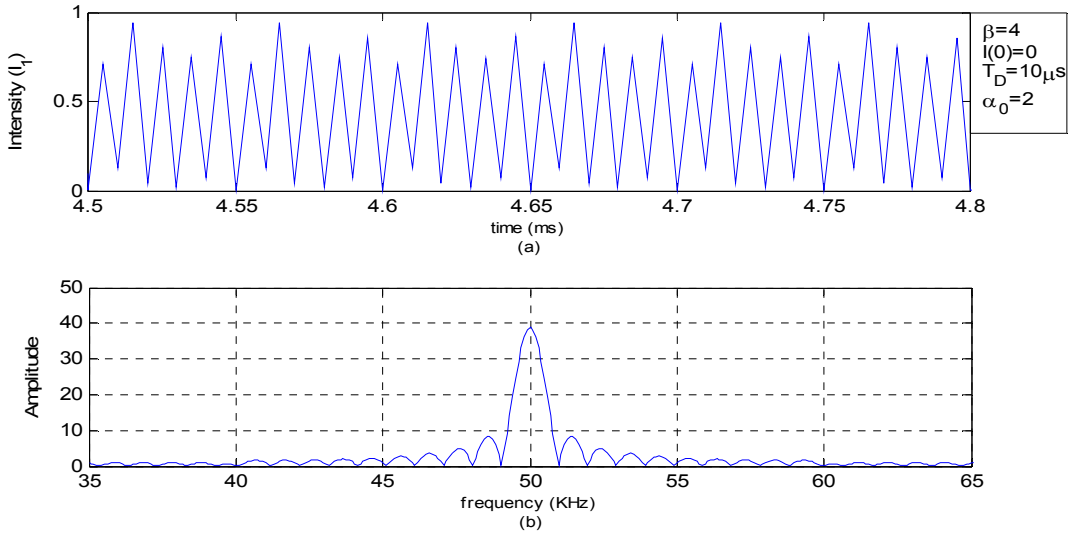

Fig.10. Chaotic wave data for (a) snapshot of time waveform, and (b) the Fourier transform.

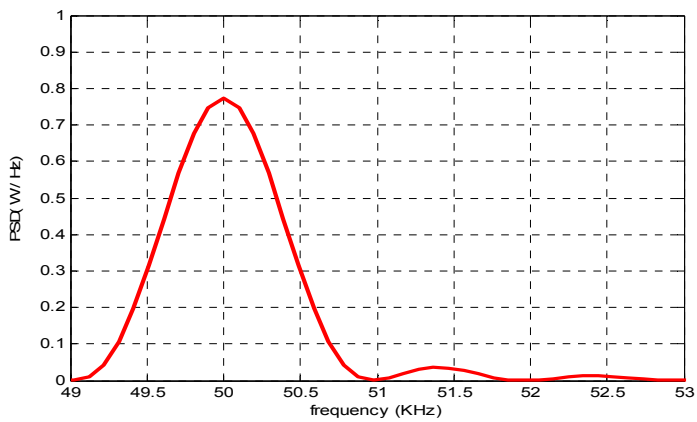

Fig.11. Chaotic wave PSD for $\tilde{\beta}$ = 4, $\hat{\alpha}_0$ = 2, I_{inc} =1, and TD = 10μs.

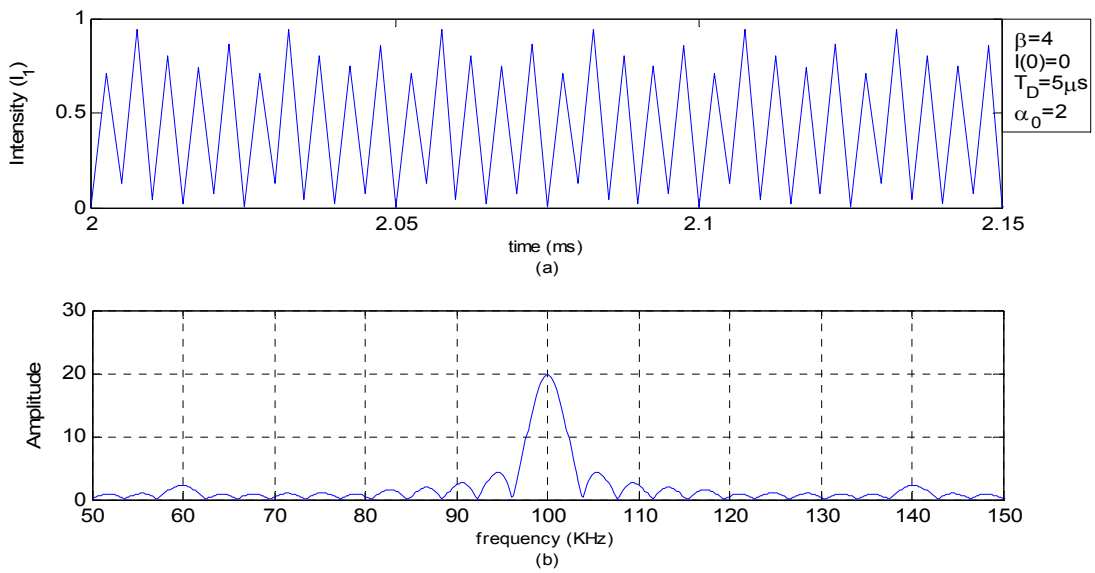

Fig.12. Chaotic wave data for (a) snapshot of time waveform, and (b) the Fourier transform.

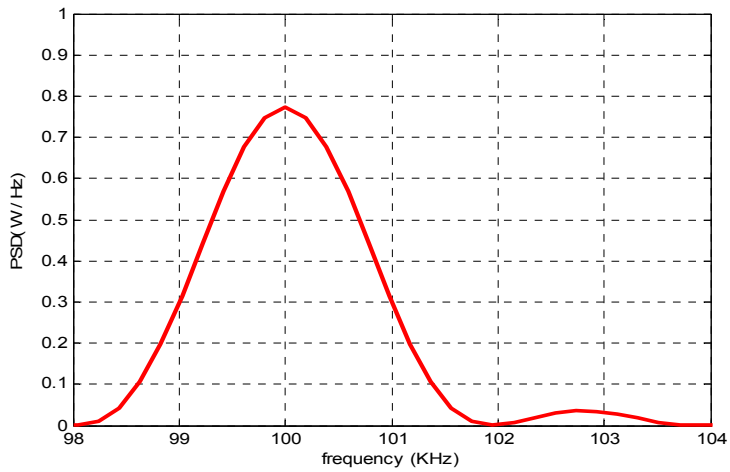

Fig.13. Chaotic wave PSD for $\tilde{\beta}$ = 4, $\hat{\alpha}_0$ = 2, I_{inc} =1, and TD = 5μs.

4. TURBULENCE POWER SPECTRAL DENSITY

In this part, the aim is to estimate the PSD of the atmospheric turbulence using the diffracted intensity profiles at the output plane repeated over discrete time intervals. From each time sample, an average intensity is computed. The process is repeated over a selected number of intervals (say 1000), whereupon the resulting average intensity is plotted versus time. The Fourier transform of this time snapshot of intensity is a measure of the PSD of the turbulence provided that the incident optical wave propagating through the input aperture is equivalent to a point source (i.e., the aperture is treated as an ideal pinhole). In the first series, the PSD is computed under different atmospheric turbulence conditions (weak, moderate, and strong) by placing the phase screen midway between the source and the screen. In the second series, the turbulence is assumed to be moderate, and the PSD is calculated at two different phase screen positions (z = 0 and z = L). In order that the observed time plot and its Fourier transform reflect the PSD characteristics of the turbulence, advantage is taken of the fact that the turbulent system may be regarded as linear. Therefore, the output (spatial) spectrum is readily described as the product of the input spectrum and the equivalent transfer function of the system. Hence, assuming propagation of either a point source or an optical wave through a pinhole leads to an input spectrum that is spatially uniform. Therefore, the resulting diffracted spectrum is a direct measure of the PSD of the turbulent system. The spatial spectral data is thereafter converted into time data by evaluating the average spatial spectra over discrete time intervals. The parameters used for the calculations are: grid size = 500mm x 500 mm; grid resolution = 512x512 pixels; total propagation distance L = 5 km; point source function exiting aperture plane= $\delta(x_0)\delta(y_0)$ in the transverse input plane x_0 and y_0 ; inner scale l_o= 1mm; and outer scale L_o = 1 km.

In pursuing the derivation of the time waveform and the corresponding PSD of the turbulence, as was mentioned, 1000 spectral samples have been used (via discrete time iterations) for each case. For each iteration, we calculate the intensity within the square window centered at origin of the grid (widow size=100x100 pixels), the total time for time waveform is adjusted to be 100 seconds (thus a time interval of 0.1 sec.). After we find the time waveform, we follow the same procedure as in section 3.2 to calculate the PSD.

4.1 Atmospheric turbulence strength

As discussed, the random phase screen is placed at the halfway point along the propagation distance and the field is evaluated at the observation plane. All other parameters mentioned above are kept constant except for the structure parameter C_n^2 (or r_0) which characterizes the strength of the turbulence.

a) Weak turbulence (r_0= 10mm or C_n^2=1.067x10^{-18} m$^{-2/3}$)

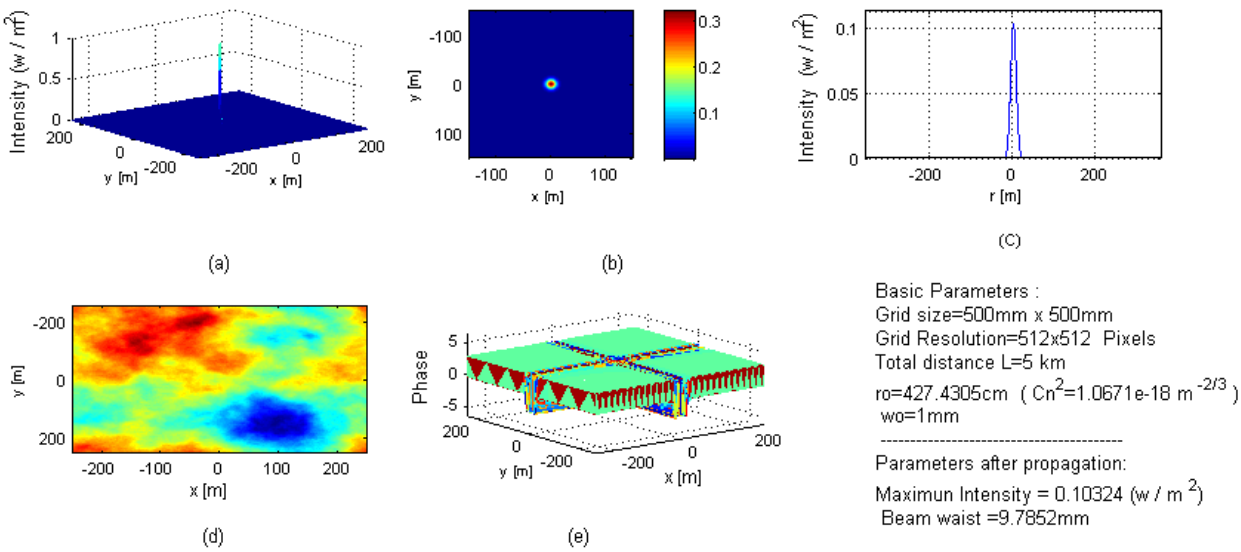

Fig.14. Point source propagation to distance z = L. (a) 3D point source; (b) transverse plane intensity distribution at z = L, (c) 2D intensity profile, (d) random phase screen distribution profile, and (e) 3D field phase angle distribution in output plane.

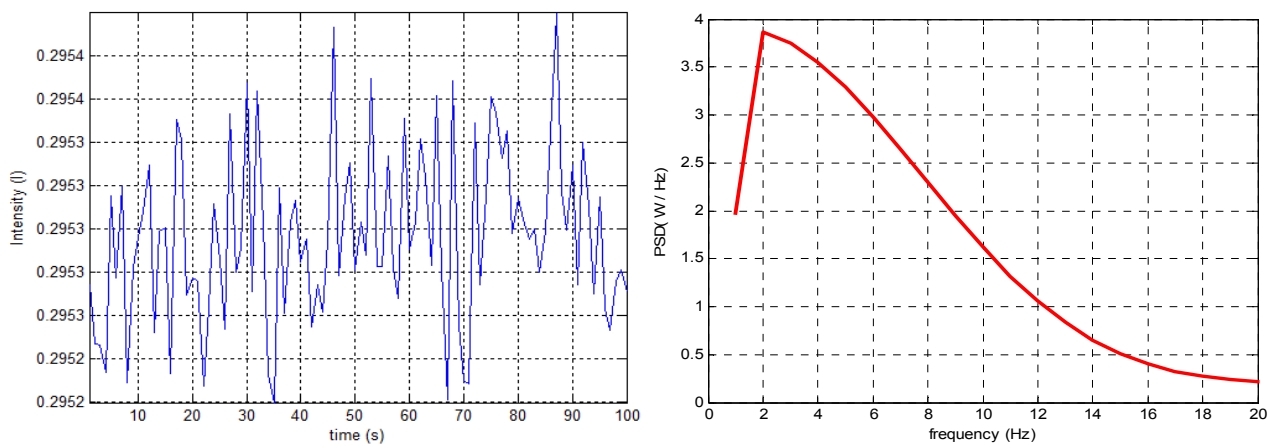

(a) (b)

Fig.15. (a) Time snapshot of the average spatial turbulence intensity, and (b) PSD of turbulence derived from spectrum shown in (a).

(b) Moderate turbulence (r_0= 0.1 mm or C_n^2=2.299x10^{-15} m$^{-2/3}$)

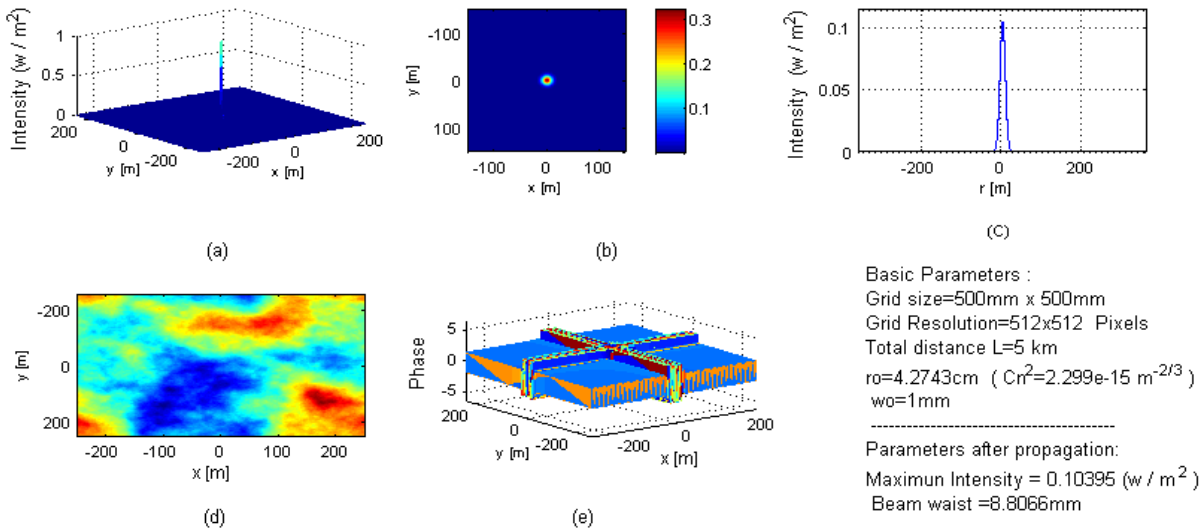

Fig.16. Point source propagation to distance z = L. (a) 3D point source; (b) transverse plane intensity distribution at z = L, (c) 2D intensity profile, (d) random phase screen distribution profile, and (e) 3D field phase angle distribution in output plane.

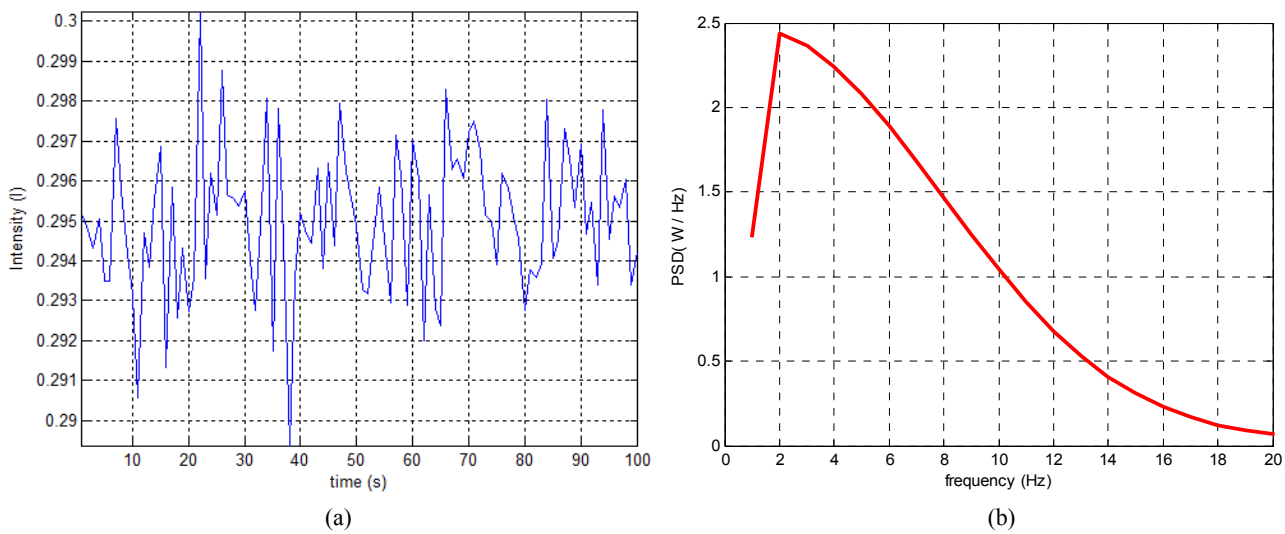

Fig.17. (a) Time snapshot of the average spatial turbulence intensity, and (b) PSD of turbulence derived from spectrum shown in (a).

c) Strong turbulence (r_0= 0.01mm or C_n^2=1.067x10^{-13} m$^{-2/3}$)

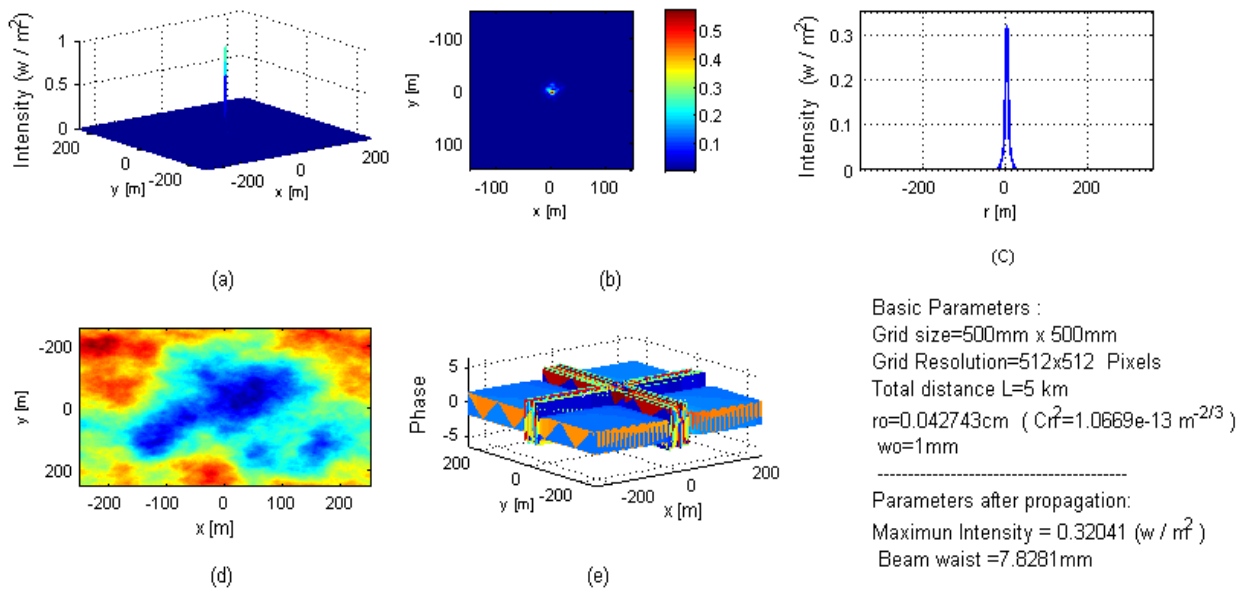

Fig.18. Point source propagation to distance z = L. (a) 3D point source; (b) transverse plane intensity distribution at z = L, (c) 2D intensity profile, (d) random phase screen distribution profile, and (e) 3D field phase angle distribution in output plane.

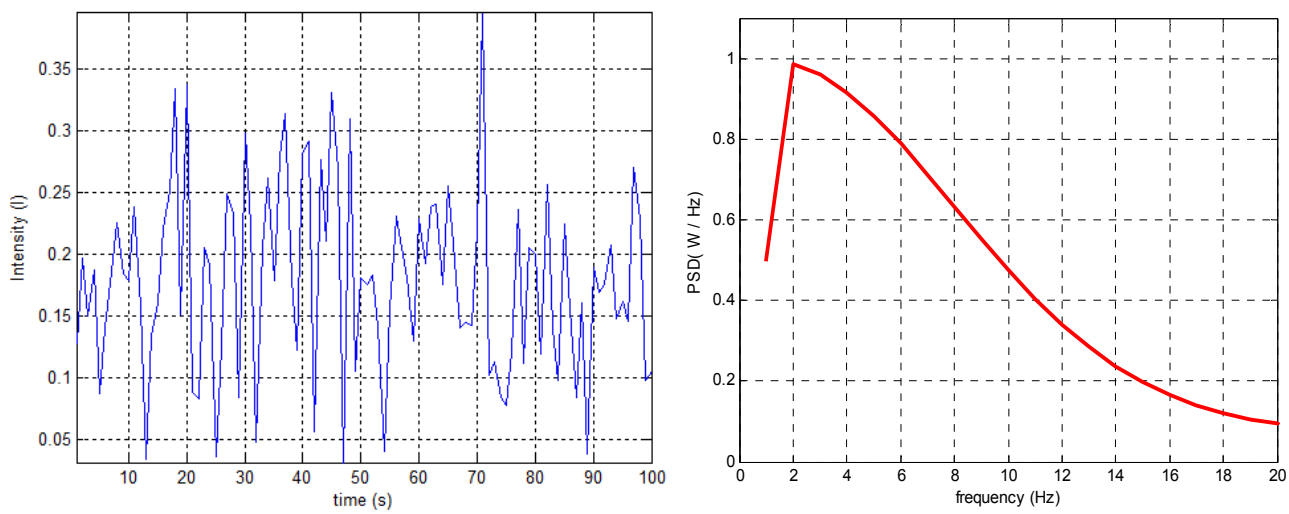

Fig.19. (a) Time snapshot of the average spatial turbulence intensity, and (b) PSD of turbulence derived from spectrum shown in (a).

From Figs.14, 16, and 18, point source excitation has little impact by way of the intensity spectrum for different turbulence strengths, except for the amplitudes seen in the PSD plots of Figs. 15(b), 17(b) and 19(b). The latter figures indicate an amplitude lowering (from about a peak of 3.8 to 0.95) as the turbulence changes from weak to strong. This makes sense intuitively, since higher turbulence implies greater attenuation and scattering of the EM wave. The PSD in all cases appears to be strongest around a rather low frequency (about 2 Hz); however, this is simply related to the time scale (or interval) over which the scattered intensity is measured. Reducing the time interval is likely to increase this frequency.

4.2 Phase screen position

In this part, we assume moderate turbulence (r_0 = 0.1 mm or C_n^2=2.299x10^{-15} m$^{-2/3}$) and hold all other parameters constant. The random phase screen is located at the beginning and at the end of the propagation path. The PSD of the field is evaluated from measurements in the image plane.

a) Phase screen at z = 0

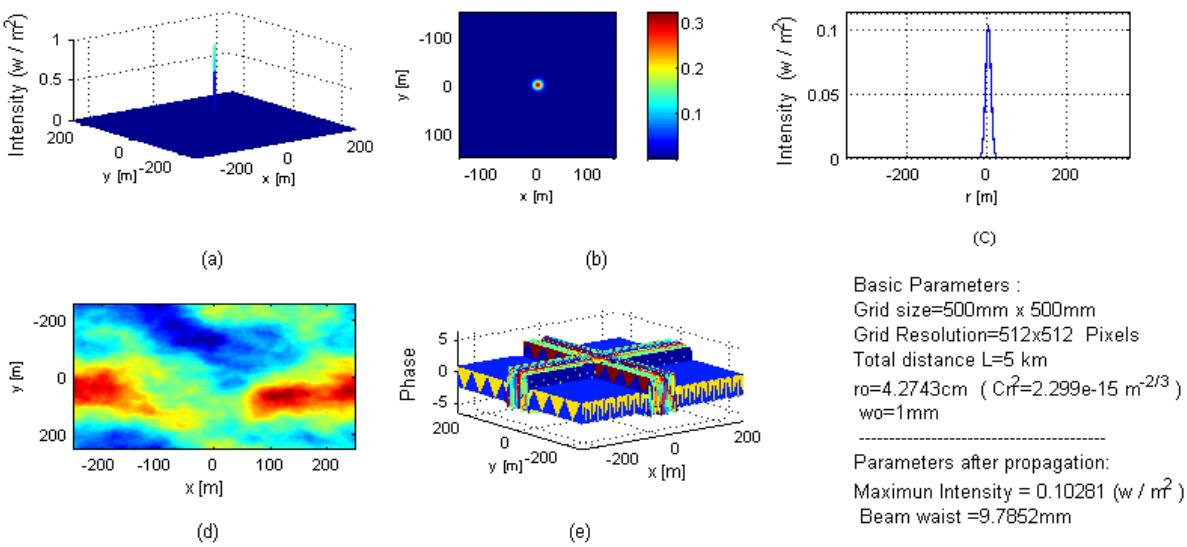

Fig.20. Point source propagation to distance z = L. (a) 3D point source; (b) transverse plane intensity distribution at z = L, (c) 2D intensity profile, (d) random phase screen distribution profile, and (e) 3D field phase angle distribution in output plane.

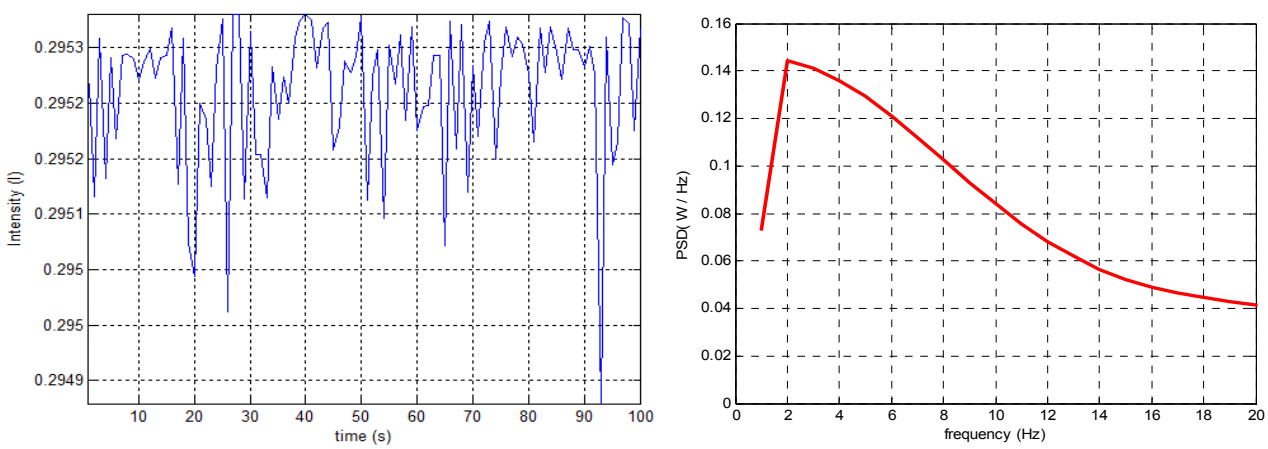

Fig.21. (a) Time snapshot of the average spatial turbulence intensity, and (b) PSD of turbulence derived from spectrum shown in (a).

b) Phase screen at z = L

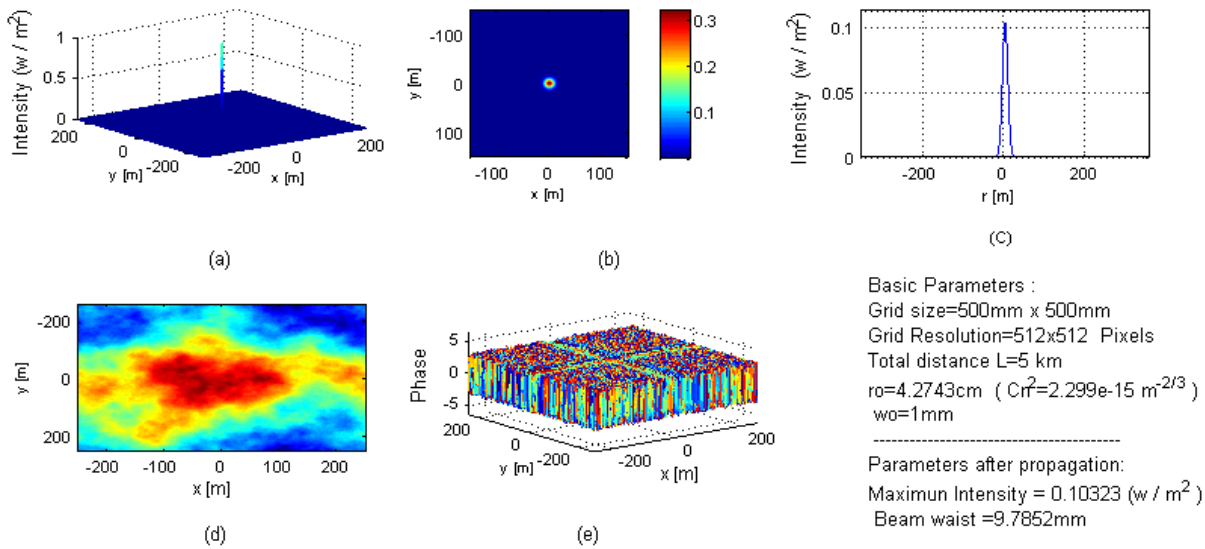

Fig.22. Point source propagation to distance z = L. (a) 3D point source; (b) transverse plane intensity distribution at z = L, (c) 2D intensity profile, (d) random phase screen distribution profile, and (e) 3D field phase angle distribution in output plane.

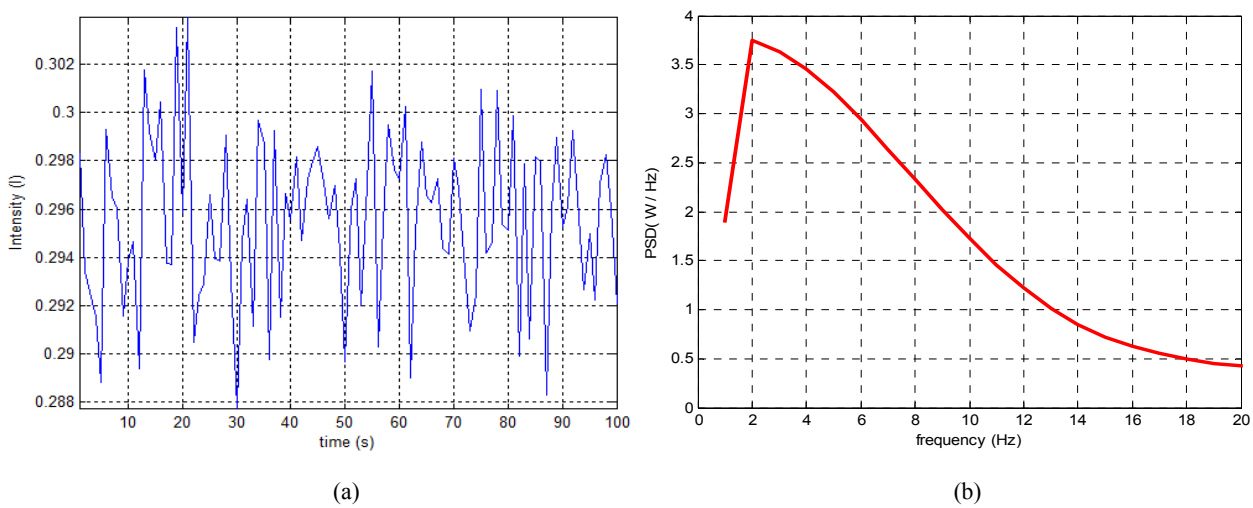

Fig.23. (a) Time snapshot of the average spatial turbulence intensity, and (b) PSD of turbulence derived from spectrum shown in (a).

There is effectively no difference between the figures 21(b) and 23(b) except for a much lower amplitude for the case where the phase screen is at z = 0 (so that the field propagates through the turbulence much earlier and then diffracts to the position L) than when it is placed at z = L (for very similar reasons).

5. CONCLUDING REMARKS

It is known that as an electromagnetic (EM) wave propagates through the atmosphere, turbulence induces amplitude and phase fluctuations. In this paper, propagation of EM waves is considered in relation to two types of random processes, viz. the case of EM propagation of chaotic waves (which may or may not be modulated), and the case of propagation through a region of narrow atmospheric turbulence. The PSD is derived using a Fourier transform approach in each case. For the PSD of the chaotic wave, time waveforms of the chaotic photocurrent and their Fourier spectra are obtained over a number of time intervals, and from the average spectral intensities, the PSD is estimated for different feedback time delays. For the case of the narrow phase turbulence, diffracted field intensities were numerically found in the image plane using the von Karman model. For a given turbulence strength and phase screen placement, these intensity plots were computed over a large number of time intervals, and then the average intensities were plotted versus time. The PSD was then evaluated using the Fourier transform of the time plots of the average intensity. For the chosen values of feedback time delays and the turbulence time intervals, the resulting PSDs appear to have profiles over very different frequency bands. Propagation of EM waves in the presence of both types of random processes and for different turbulence and delay conditions will require further investigation.

REFERENCES

[1] L. C. Andrews and R. L. Phillips, *Laser Beam Propagation through Random Media*, 2nd ed. Bellingham: SPIE Press, 2005.

[2] X. Zhu and J.M. Kahn, "Free-space optical communication through atmospheric turbulence channels," IEEE Trans. Comm., vol. 50, No. 8, Aug. 2002.

[3] A. N. Kolmogorov, "The Local Structure of Turbulence in Incompressible Viscous Fluid for Very Large Reynolds Numbers," Proceedings: Mathematical and Physical Sciences, vol. 434, pp. 9-13, 1991.

[4] A. N. Kolmogorov , " A refinement of previous hypotheses concerning the local structure of turbulence in a viscous incompressible fluid at high Reynolds number," J. Fluid Mech., vol. 13, pp. 82, 1962.

[5] A. M. Obukhov, "On the distribution of energy in the spectrum of turbulent flow," Dokl. Akad. Nauk SSSR, vol. 32, pp. 22-24, 1941.

[6] V. I. Tatarskii, *Wave Propagation in a Turbulent Medium*. New York: McGraw-Hill, 1961.

[7] A. Ishimaru, *Wave Propagation and Scattering in Random Media*. New York: IEEE Press, 1997; 1978.

[8] J. W. Strohbehn and S. F. Clifford, *Laser Beam Propagation in the Atmosphere*. Berlin; New York: Springer Verlag,1978.

[9] E.M. Whitfield, P.P. Banerjee and J.W. Haus, "Propagation of Gaussian beams through a modified von Karman phase screen," Proc. SPIE, vol. 8517, pp.85170-1-7, Oct. 2012.

[10] A.K. Majumdar, Department of the Navy, China Lake, CA. Private communication.

[11] A. Korpel, , *Acousto-Optics*, 2nd edition (Marcel Dekker, New York, 1997).

[12] P. Debye and F. W. Sears, "On the scattering of light by supersonic waves," Proc. Nat. Acad. Sci. 18, 409-414 1932.

[13] A. Cont, T. C. Poon, "Simulations of Bistable Acousto-Optic Devices Using MATLAB", Proc. IEEE, 2003.

[14] W.L. Bragg, " The Diffraction of Short Electromagnetic Waves by a Crystal," Proc. Camb. Phil. Soc. 17, 43-75 1913.

[15] B. E. A. Saleh, M. C. Teich, "*fundamentals of photonics*", 2nd ed., New Jersey, USA, 2007.